Lord, O. T., Walter, M. J., Dobson, D. P., Armstrong, L. S., Clark, S. M., & Kleppe, A. (2010). The FeSi phase diagram to 150 GPa. Journal of Geophysical Research: Solid Earth, 115(6), [B06208]. DOI: 10.1029/2009JB006528

JOURNAL OF GEOPHYSICAL RESEARCH, VOL. 115, B06208, doi:10.1029/2009JB006528, 2010

The FeSi phase diagram to 150 GPa

O. T. Lord,[1] M. J. Walter,[1] D. P. Dobson,[2] L. Armstrong,[1] S. M. Clark,[3] and A. Kleppe[4]

Received 9 April 2009; revised 26 November 2009; accepted 29 January 2010; published 23 June 2010.

[1] The melting curve of FeSi has been determined to 150 GPa in the laser-heated diamond anvil cell (LH-DAC) on the basis of discontinuities in the power versus temperature function. A multianvil experimental cross-check at 12 GPa using textural criteria as a proxy for melting is in good agreement with our LH-DAC results. The melting point of FeSi reaches ~4000 K at the core mantle boundary and an extrapolated value of 4900 K at the inner-core boundary (ICB). We also present the melting curve as determined by the Lindemann melting law; this agrees well with our experimental curve to 70 GPa and then diverges to higher temperatures, reaching 6200 K at the ICB. These temperatures are substantially higher than previous LH-DAC determinations. The boundary of the ε-FeSi → CsCl-FeSi subsolidus transition has also been determined by synchrotron-based X-ray diffraction at high pressures, and the results confirm a negative Clapeyron slope for the transition. We conclude that if present, FeSi is likely to be solid within the D″ layer and is unlikely to be present within the inner core for any plausible bulk core silicon content.

Citation: Lord, O. T., M. J. Walter, D. P. Dobson, L. Armstrong, S. M. Clark, and A. Kleppe (2010), The FeSi phase diagram to 150 GPa, *J. Geophys. Res.*, *115*, B06208, doi:10.1029/2009JB006528.

1. Introduction

[2] Silicon has been a popular candidate for part of the light element budget of the Earth's core [e.g., *Poirier*, 1994; *Allègre et al.*, 1995] because of its abundance and ubiquity within the silicate Earth and its known solubility in liquid iron at 1 atm (20.5 wt % Si at the eutectic [*Lacaze and Sundman*, 1991]). At conditions of high temperature and pressure, Si has been shown to have significant solubility in liquid iron in equilibrium with forsteritic melt [*Gessman et al.*, 2001], (Mg,Fe)SiO_3 perovskite [*Takafuji et al.*, 2005] and postperovskite [*Sakai et al.*, 2006], as well as in solid iron [e.g., *Kuwayama et al.*, 2009; *Lin et al.*, 2009]. A Si reservoir within the Earth's core may also help to explain the superchondritic Mg-Si ratio of the upper mantle [*Allègre et al.*, 1995] and the nonchondritic Si isotope composition of the silicate Earth [*Georg et al.*, 2007; *Shahar et al.*, 2009], although this latter proposition has been questioned [*Fitoussi et al.*, 2009].

[3] Recently, a high-pressure phase transition between B20 structured ε-FeSi and a new CsCl structured phase was predicted using ab initio calculations [*Vocadlo et al.*, 1999] and confirmed by experimental synthesis in the multianvil [*Dobson et al.*, 2002]. As is the case for ε-FeSi [*Caracas and Wentzcovitch*, 2004], the equation of state (EOS) of this new polymorph [*Dobson et al.*, 2003] suggests that a mixture of Fe and FeSi could reproduce the bulk modulus and density of the inner core derived from the preliminary reference Earth model (PREM [*Dziewonski and Anderson*, 1981]). However, recent laser-heated diamond anvil cell (LH-DAC) experimental data suggest that at inner core conditions, for any likely bulk core Si content, the solubility of Si in hcp-structured Fe is sufficient to preclude the presence of this phase in the inner core [e.g., *Kuwayama et al.*, 2009; *Lin et al.*, 2009]. Even so, assuming these EOS results can be extrapolated to the liquid state [*Dobson et al.*, 2003], Si could also form a significant part of the light element budget of the outer core, as suggested by *Badro et al.* [2007] on the basis of high-pressure sound velocity measurements on a range of Fe-rich compounds, including FeSi. This possibility has been bolstered by the determination of the EOS of Fe-rich Fe-Si alloy [*Lin et al.*, 2003], which yields densities close to those predicted by the PREM model at both inner and outer core conditions.

[4] Despite the arguments against the presence of FeSi as a stable phase in the inner core, the study of this material is relevant for several important reasons. First, the intermediate density of FeSi between that of the core and mantle have led to the phase being proposed as a component of the D″layer, to help explain the negative compressional (V_p) and shear (V_s) velocity anomalies within this region [*Caracas and Wentzcovitch*, 2004]. This suggestion is made plausible by the expectation that FeSi should form as a reaction product between the Fe-Ni outer core liquid and the (Mg,Fe)SiO_3 perovskite or postperovskite of the lower mantle should such reactions occur under the prevailing conditions [*Knittle and Jeanloz*, 1991; *Goarant et al.*, 1992]. According to *Kuwayama et al.* [2009], hcp-Fe containing 9.9 wt % Si

[1]Department of Earth Sciences, University of Bristol, Bristol, UK.
[2]Department of Earth Sciences, University College London, London, UK.
[3]Advanced Light Source, Lawrence Berkeley National Laboratory, Berkeley, California, USA.
[4]Diamond Light Source Ltd., Didcot, UK.

0148-0227/10/2009JB006528

breaks down to a Si-poor Fe alloy plus CsCl-FeSi at high temperatures. The Clapeyron slope of this transition is positive, reaching 3000 K at the core-mantle boundary (CMB) pressure of 135 GPa. This temperature is low enough to allow solid FeSi to be present on the core side of the CMB and possibly on the mantle side also, depending on the mantle geotherm and the melting curve. Because of these possibilities, the high-pressure melting curve and subsolidus phase diagram of FeSi are directly relevant to the CMB region. Second, the high-pressure phase diagram of FeSi will help to constrain the topology of the Fe-rich portion of the Fe-Si system, which is important in determining the distribution of Si within the core and lower mantle at the present day and during core formation [*Dobson et al.*, 2002; *Santamaría-Pérez and Boehler*, 2008]. Third, melting data on Fe light element compounds such as FeSi can be used to test and constrain thermodynamic models of core liquids [e.g., *Helffrich and Kaneshima*, 2004]. Finally, the data presented here are a further test of the efficacy and accuracy of the laser power versus temperature function as a melting criterion in LH-DAC experiments at conditions relevant to the lower mantle and core [*Lord et al.*, 2009].

[5] To this end, we have measured the melting curve of FeSi up to 150 GPa and mapped the position of the ε-FeSi → CsCl-FeSi phase transition by synchrotron X-ray diffraction (XRD), both in the LH-DAC. As a further experimental test of our LH-DAC melting criterion, we have performed two multianvil quench experiments at 12 GPa to bracket the melting curve using ex situ textural evidence.

2. Experimental

[6] Melting and synthesis experiments were conducted in symmetric LH-DAC with 200- to 700-μm culets. Samples were loaded into 80- to 120-μm holes drilled in stainless steel gaskets preindented to ~50-μm thickness. Starting materials consisted of 10- to 20-μm thick precompressed foils made from powdered ε-FeSi (Alpha Aesar Chemical Co.) with 99.9% purity. All starting materials were stored in an oven at ~125°C for at least 1 h before loading to reduce moisture within the assembly. Foils were loaded into the LH-DAC between insulating layers, which also acted as the pressure medium. A range of pressure media were used, including NaCl, single-crystal sapphire discs, and foils of ruby, but in the majority of experiments, these layers consisted of form-fitting discs of nanocrystalline Al_2O_3 [*Lord et al.*, 2009].

[7] Pressure was monitored during compression using the fluorescence signal from a thin layer of submicron ruby powder smeared across the upper insulating layer, as calibrated by *Mao et al.* [1986]. This allows pressure to be measured wherever melting takes place and pressure gradients across the entire sample chamber to be monitored; these did not usually exceed 2 GPa, though on two occasions, gradients of up to 8 GPa were measured. The spatial location of melting was carefully recorded during the experiment, and the reported melting pressure is the mean of several measurements around this location. The uncertainty in the reported pressures is thus the sum of the standard deviation in the measured pressures and the analytical uncertainty in the ruby fluorescence measurement itself, which increases with pressure and is estimated as ±1–2 GPa. We assume that the postheating pressure represents a minimum estimate of the pressure at melting and do not make any attempt to correct for the effect of thermal pressure in our experiments.

[8] Samples were heated in a double sided-heating geometry using a 100 W Nd:YAG CW diode-pumped multimode laser, producing stable spots 30–50 μm in diameter. Temperatures were measured spectroradiometrically on one side using standard techniques employed at Bristol and described in detail elsewhere [*Lord et al.*, 2009; *Walter and Koga*, 2004]. In most cases, the measurement precision as determined by the closeness of the fit of the measured spectra to the greybody Wien function is on the order of 3–7 K and does not exceed 13 K at the highest temperatures measured in this study (~4000 K). This uncertainty does not include deviations in emissivity from the idealized greybody behavior assumed in the measurement. Based on a 1 atm melting point calibration of Pt, Nb, Mo, Ta, Re, and W, this may result in an overestimation of temperature on the order of 50–200 K [*Lord et al.*, 2009]. However, we make no attempt to assign any formal uncertainty in accuracy to our measurements. As temperature increases, the Wien approximation begins to underestimate temperature compared to the Planck function. However, even at the highest temperatures recorded in this study (~4000 K), the discrepancy is <25 K.

[9] Melting was determined by the detection of discontinuities in the temperature versus laser power function. This melting criterion is based on the concept that the temperature should plateau at an endothermic invariant melting point as the laser power provides the latent heat of melting [e.g., *Boehler et al.*, 1990; *Lazor et al.*, 1993; *Shen et al.*, 1993; *Dewaele et al.*, 2007]. Several examples of the power-temperature relationship from typical melting experiments are shown in Figure 1. Temperature rises monotonically and linearly as laser power is increased until the melting point is reached, at which point the temperature plateaus. The melting temperature is taken as the average of the measured temperatures within the plateau. The reported uncertainty in the melting temperature is taken as the sum of the uncertainty in the position of the plateau (10–50 K), the analytical uncertainty (3–13 K), and the estimated temperature gradient within the hot portion of the heated spot (~30 K).

[10] Subsolidus LH-DAC synthesis experiments were heated at their target pressure and temperature for 20–60 min while being moved at regular intervals to ensure annealing of the entire sample. XRD analysis of the heated samples at pressure in the LH-DAC was carried out at beam-line I15 of the diamond light source (DLS) using a wavelength of 0.438–0.536 Å and beam-line 12.2.2 of the advanced light source (ALS) using a wavelength of 0.444 Å. Samples were exposed for 120–600 s, with 2D diffraction patterns collected using a Mar345 image plate. The sample to detector distance was calibrated using a Si standard (DLS) or a LaB_6 standard (ALS). The 2D diffraction patterns were integrated into 1D spectra using the FIT2D program [*Hammersley*, 1997].

[11] As an independent experimental cross-check of our LH-DAC melting criterion, we carried out multianvil

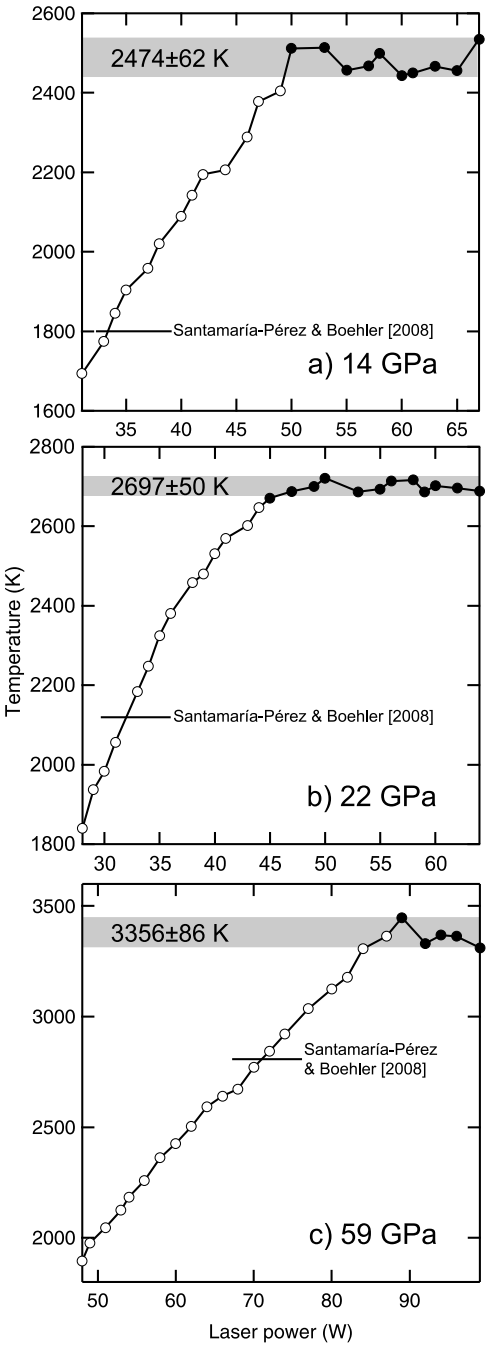

Figure 1. Typical laser power versus temperature functions acquired during laser heating of FeSi at (a) 14 GPa, (b) 22 GPa, and (c) 59 GPa. Each point represents a spectroradiometric temperature measurement for which the precision is less than the symbol size (3–5 K). The melting temperature is determined from the mean of the points within the plateau (filled circles). The expected melting temperatures from the work of *Santamaría-Pérez and Boehler* [2008] are denoted by the horizontal lines. See section 2 for an explanation of the reported uncertainties in the melting temperatures (shaded bars).

melting experiments at 12 GPa and temperatures of 2100 K and 2300 K using a 14/8 assembly at the Beyerisches Geoinstitut, Bayreuth, Germany. Angular chips of FeSi were loaded into a powdered Al_2O_3 pressure medium within an MgO capsule, which was in turn loaded directly into a $LaCrO_3$ furnace. A D-type W/Re thermocouple was located coaxially but separated from the sample volume with a 150-μm Al_2O_3 disc and offset by ~1 mm from the furnace hot spot where the sample was located. On the basis of cell calibrations [*Mossenfelder et al.*, 2000], uncertainties in sample pressure and temperature are ±1 GPa and ±100 K, respectively. Experiments were heated to the desired temperature, held for several minutes, and quenched by shutting off the power. After decompression, the capsules were broken open to reveal the sample, and melting was determined from the shape and texture of the sample. As discussed below, the melting bracket from these experiments is in good agreement with our LH-DAC melting data.

3. Results

3.1. FeSi Phase Relations to 150 GPa

[12] Figure 2 shows subsolidus and melting phase relations for FeSi. Our diffraction results indicate a steep and negative slope for the subsolidus phase transition boundary between the ε-FeSi and CsCl-FeSi polymorphs, as expected from the multianvil experiments of *Dobson et al.* [2002]. Figure 3 shows two typical diffraction patterns from subsolidus experiments acquired at pressure after laser heating. In an experiment at 10 GPa and 1790 K (Figure 3a), all the peaks index to ε-FeSi or the Al_2O_3 pressure medium. At 30 GPa and 1900 K (Figure 3b), new peaks appear, which index to the high-pressure CsCl-structured phase of FeSi based on the known space group ($P2_13$) and unit cell parameters derived from the room temperature EOS [*Dobson et al.*, 2003]. The majority of the diffraction results can be satisfied by a linear phase boundary of the form

$$P = -0.0551\mathrm{T} + 121.6.$$

The exception is a point at 13 GPa and 1800 K (Figure 2b), which is the result of a failed reversal attempt. This experiment was previously annealed at 13 GPa and 2050 K and the high-pressure polymorph formed. However, we were unable to fully transform back to the low-pressure phase on laser heating at 13 GPa and 1800 K. Only in one case, at 46 GPa and 1830 K, did the transition run to completion, yielding pure CsCl-FeSi. The metastable persistence of ε-FeSi on the high-pressure side of the phase boundary is possibly due to kinetic inhibition caused by the substantial predicted activation barrier of the reaction [*Vocadlo et al.*, 1999] and may explain why previous workers failed to find the transition at lower temperatures [*Knittle and Williams*, 1995; *Lin et al.*, 2003].

[13] The subsolidus reaction boundary intersects the melting curve at ~5 GPa and 2100 K. The intersection of the univariant subsolidus phase transition with the two univariant melting curves (ε-FeSi = melt and CsCl-FeSi = melt) must produce an inflection along the solidus, although it may not be large. Our melting data are not sufficiently precise to constrain the magnitude of the inflection on a P-T

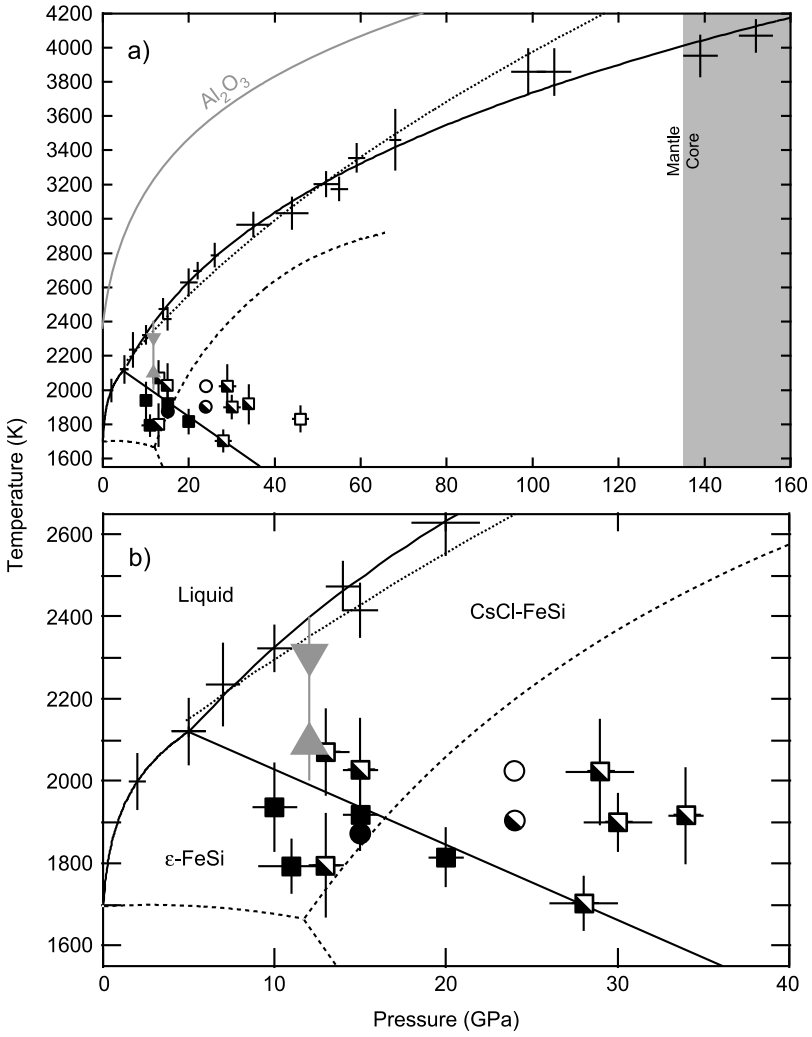

Figure 2. (a) The FeSi phase diagram as determined from laser-heated diamond anvil cell (LH-DAC) melting experiments (crosses) and X-ray diffraction (XRD) synthesis experiments (ε-FeSi, filled squares; CsCl-FeSi, open squares; both phases, divided squares). The results of a single melting bracket at 12 GPa in the multianvil are also plotted (shaded triangle, solid; shaded inverted triangle, liquid). The results of a previous multianvil synthesis study by *Dobson et al.* [2002] analyzed by ex situ XRD are indicated by the circles (color coding as above). The solid lines are phase boundaries; the melting line is determined by a fit to the data using the empirically derived Simon equation. The dashed line indicates the melting line determined by the LH-DAC in *Santamaría-Pérez and Boehler* [2008], using the observation of melt motion with the aid of the laser speckle technique as a melting criterion. The subsolidus line emanating from the triple point represents one of the possible phase boundaries proposed by *Santamaría-Pérez and Boehler* [2008]. The dotted line is the melting curve of the high-pressure phase as predicted using the Lindemann melting law. The melting curve of the Al_2O_3 pressure medium from *Shen and Lazor* [1995] is shown for comparison. (b) The low-pressure region expanded from Figure 2a. All experiments used Al_2O_3 as a pressure medium, except the subsolidus data at 20, 34, and 46 GPa, which used NaCl.

diagram. However, when the melting data are fitted as a function of Eulerian finite strain (Kraut-Kennedy equation), an inflection is evident at a pressure close to the pressure at which the subsolidus curve intersects the melting curve (Figure 4).

[14] The melting curve on Figure 2 shown as a solid line is based on a fit to the Simon equation, with data below and above the transition fitted separately. We have also calculated the melting curve using the Lindemann law [*Anderson and Isaak*, 2000]:

$$T_m = (V/V_0)^{2/3} \exp(2\gamma_0/q(1-(V/V_0)^q)) \times T_{m0},$$

where $\gamma_0 = 2.33$ is the Grüneisen parameter for CsCl-FeSi taken from *Vocadlo et al.* [2002], which is in good agreement with the value of 2.04 ± 0.39 determined from the

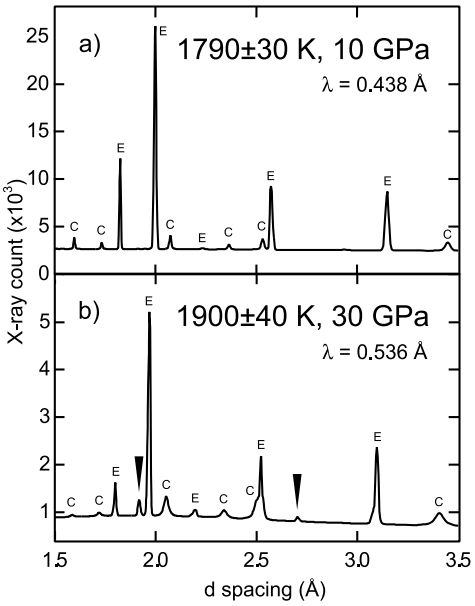

Figure 3. Examples of XRD patterns from LH-DAC synthesis experiments on FeSi at high pressure and room temperature after quenching. (a) After heating at 1790 ± 30 K and 10 GPa, all the peaks index to either the low-pressure ε-FeSi phase (indicated by E) or the Al_2O_3 pressure medium (indicated by C). (b) After heating at 1900 ± 40 K and 30 GPa, new peaks, diagnostic of the high-pressure CsCl-type polymorph, are evident (arrows).

fitting parameters of the Kraut-Kennedy equation to the melting data in this study. We assume the volume dependence of the Grüneisen parameter, $q = 1$ [*Boehler et al.*, 2000]. Because of the lack of high-temperature EOS data for CsCl-FeSi, the volume at melting at 1 atm (V_0) and at high pressure (V) is calculated using the temperature-independent thermal expansion coefficient of 5.1×10^{-5} measured for ε-FeSi [*Guyot et al.*, 1997]. T_{m0} is the fictive 1 atm melting point of the high-pressure phase as determined from the fitting parameters of the Kraut-Kennedy equation. The resulting Lindemann Law melting curve closely follows the Simon fit to the measured data to ~70 GPa, at which point it diverges to higher temperatures, reaching ~4400 K at the CMB (135 GPa) and ~6200 K at the ICB (330 GPa). This compares to ~4000 K at the CMB and an extrapolated value of ~4900 K at the ICB on the basis of the Simon fit to our data. The reason for the divergence between the calculated and measured melting curves above 70 GPa is not known but is presumably the result of inaccuracies and oversimplifications in the assumed thermal parameters of the CsCl-FeSi phase, and of the fact that the Lindemann melting law only takes the thermodynamic parameters of the solid into account and neglects the liquid phase.

[15] To calibrate the accuracy of our melting results, we compare LH-DAC melting determinations for Fe, Fe_3C, and the Fe-Fe_3C eutectic to determinations made on the basis of textural analysis of quenched experiments made in piston-cylinder and multianvil presses (Figure 5). In all cases we obtain results in the LH-DAC that closely match these independent melting determinations [see also *Lord et al.*, 2009]. Further evidence for the accuracy of this method can be gleaned from the study of *Dewaele et al.* [2007] on the melting of Pb. In this study, melting was determined by several in situ XRD criteria such as the loss of diffraction lines, the onset of rapid recrystallization, and the appearance of diffuse scattering from the liquid phase but also the same power versus temperature criterion employed here. The plateaus they observed coincided with the criteria observed in their XRD patterns. *Lord et al.* [2009] reported a melting curve for Pb using the power versus temperature criterion that closely reproduces the melting curve of *Dewaele et al.* [2007]. We have also carried out melting experiments using Al_2O_3 as a pressure medium on Fe, FeS, Pt, and Pb, up to 45 GPa and 2600 K. In all cases, the measured melting points fall within 100 K of the relevant literature curve, which were all produced using softer pressure media such as NaCl and Ar in the LH-DAC [*Lord et al.*, 2009]. This close correspondence validates our melting criterion and also indicates that the thermal pressure is not significantly different when using Al_2O_3 as a pressure medium, as compared to softer media commonly used in LH-DAC experiments.

[16] As a final test of the validity of our FeSi melting curve, we bracketed the melting point at 12 GPa using a multianvil apparatus. Photomicrographs of the run products from the two multianvil melting experiments are presented in Figure 6. The congruent nature of the melting of FeSi makes determining melting by chemical means impossible, so other criteria must be used. The recovered sample from an experiment at 2100 K clearly retained its initial angular shape and is polycrystalline and fissile (Figures 6a and 6b). In contrast, the run product from an experiment at 2300 K has formed a single, rounded, and nonfissile nugget (Figure 6c), indicating that the entire sample was melted. During the 2300 K experiment, the thermocouple became unstable after 3 min. The recovered sample had clearly come into contact with the thermocouple during the experiment, triggering the instability and requiring the sample to have moved over 100 μm, which strongly suggests the sample was in

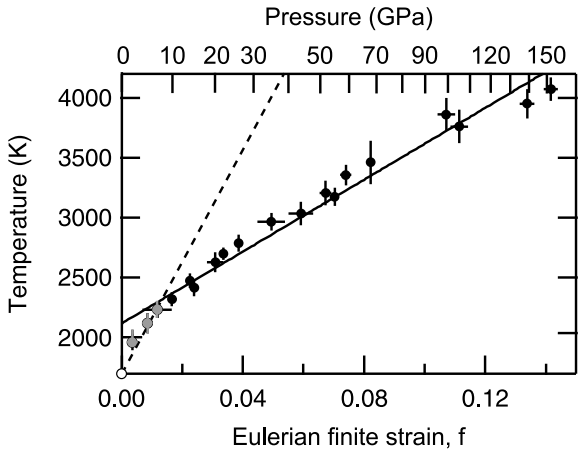

Figure 4. LH-DAC melting data for FeSi fitted to the Kraut-Kennedy equation. Eulerian finite strain is calculated using the Birch-Murnaghan equation of state with $V_{0,300}$, $K_{0,300}$, and $K'_{0,300}$ for ε-FeSi (shaded circles; dashed line) taken from *Lin et al.* [2003] and for CsCl-FeSi (filled circles; solid line) taken from *Dobson et al.* [2003].

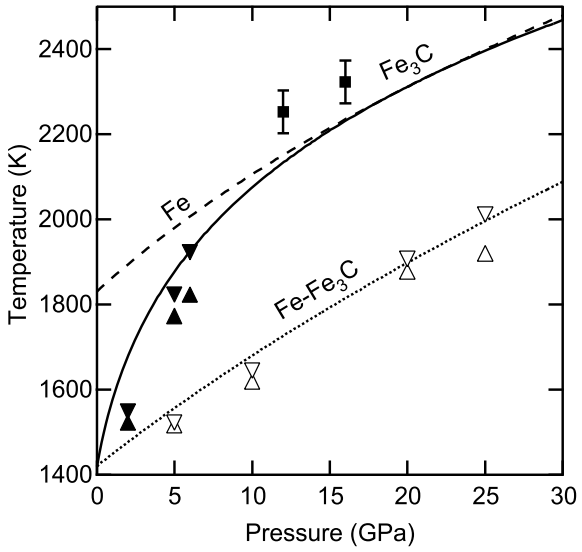

Figure 5. Examples of LH-DAC melting data corroborated with multianvil quench experiments. The melting curves for Fe, Fe_3C, and the Fe-Fe_3C eutectic [*Lord et al.*, 2009] were measured using the laser power versus temperature melting criterion in Bristol. The results of large-volume press quench experiments are presented for the Fe-Fe_3C eutectic (open triangles [*Fei et al.*, 2007]), Fe_3C (solid triangles [*Lord et al.*, 2009]), and Fe (solid squares [*Ringwood and Hibberson*, 1990]).

the liquid state. In the experiment at 2100 K, the thermocouple showed no sign of instability. These data suggest that at 12 GPa, FeSi melts between 2100 K and 2300 K, within mutual error of our LH-DAC determinations (Figure 2b).

3.2. Comparison With Previous Work

[17] *Santamaría-Pérez and Boehler* [2008] recently published a melting curve for FeSi to ~70 GPa, also using LH-DAC techniques. It is clear from Figure 2 that our melting temperatures, derived from both LH-DAC and multianvil melting experiments, are substantially higher than those of *Santamaría-Pérez and Boehler* [2008] at all pressures. At its peak near 12 GPa, the mismatch reaches 700 K, the magnitude of which is hard to explain by differences in temperature measurement techniques, which are similar in the two studies. There are two primary differences between the studies: the melting criterion and the pressure medium employed. In the case of the melting criterion, we use discontinuities in the laser power versus temperature function, whereas *Santamaría-Pérez and Boehler* [2008] looked for melt motion in the "speckle" pattern created by an argon laser [*Boehler et al.*, 1997]. Detection of melt motion could overestimate the melting point if vigorous convection occurs after a super-liquidus temperature is reached, but this does not explain the mismatch, because the melting curve of *Santamaría-Pérez and Boehler* [2008] is lower than that presented here. In the case of the pressure medium, we employed Al_2O_3, whereas *Santamaría-Pérez and Boehler* [2008] used KBr, CsCl, and KCl and saw no dependence of melting temperature on pressure medium. Reactions with the pressure medium are unlikely in this study, as we saw no extraneous peaks in diffraction patterns taken from quenched melting experiments from 2 to 68 GPa.

[18] The melting curve proposed by *Santamaría-Pérez and Boehler* [2008] is distinguished by a negative slope at pressures just below the intersection with the subsolidus ε-FeSi → CsCl-FeSi phase transition. This results in a deep cusp along the melting curve at ~12 GPa, which they attribute to the intersection of the transition with the melting curve. The negative melting slope implies a negative volume change upon melting, which could occur if the compressibility of liquid FeSi were much greater than that of the solid. We note, however, that in the case of pure iron, there is no indication of such anomalous liquid compressibility, as the melting slope is positive at least up to 200 GPa, and there is only a relatively mild cusp along the pure Fe solidus at ~60 GPa resulting from the γ to ε subsolidus transition [e.g., *Shen et al.* 1998]. Further evidence against such anomalous melting behavior comes from the work of *Sanloup et al.* [2002], who measured the radial distribution function of an Fe-17 wt% Si liquid alloy and showed that the alloy liquid displays pure Fe-like local order, and suggested that pure Fe liquids and Fe-Si alloy liquids should have very similar bulk compressibilities.

[19] Our independent determination of the melting point at 12 GPa using multianvil techniques, and the high-pressure in situ determination of the subsolidus phase transition in this study and in the study of *Dobson et al.* [2002], are inconsistent with any of the possible topological constructions around the triple point that were considered by *Santamaría-Pérez and Boehler* [2008]. For example, in the multianvil experiment at 12 GPa and 2100 K, FeSi is still solid at a temperature 400 K above the proposed melting temperature of *Santamaría-Pérez and Boehler* [2008]. Furthermore, in our LH-DAC melting experiments that were heated to temperatures well above the melting curve of *Santamaría-Pérez and Boehler* [2008], no laser power versus temperature anomalies were detected on the way to the melting temperature. As shown in Figure 1, the power-temperature

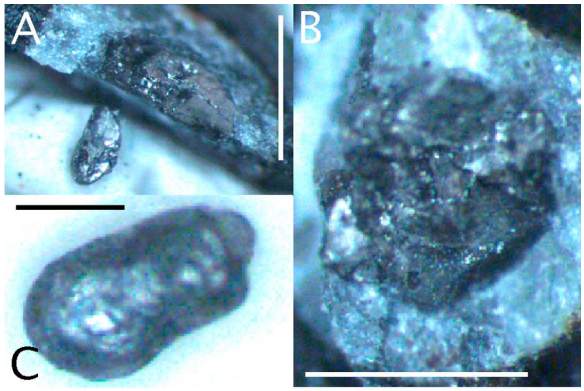

Figure 6. Photomicrographs of run products from multianvil melting experiments at (a, b) 2100 K and (c) 2300 K. It is clear that the sample quenched from 2100 K (Figures 6a and 6b) remained polycrystalline and angular where the FeSi was in contact with the capsule. The sample quenched from 2300 K formed a single smooth lump, suggesting the angular polycrystalline aggregate coalesced while molten (Figure 6c). Scale bars, 1 mm.

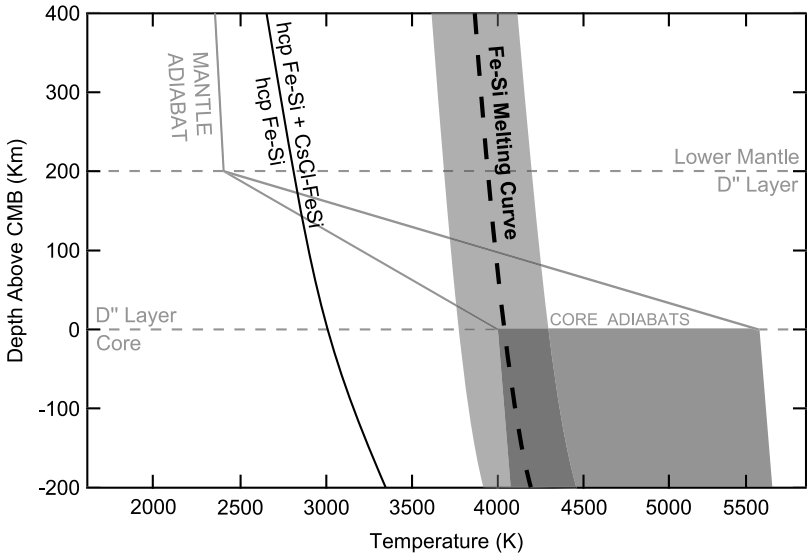

Figure 7. FeSi in the D″ layer. The solid gray line denotes the mantle adiabat [*Katsura et al.*, 2009] and the dark gray field the range of possible core adiabats [*Boehler*, 1993; *Alfè*, 2009]; the two are connected by a simplified, linear interpolation (dashed gray lines). The solid black line denotes the breakdown reaction hcp Fe-Si alloy → hcp Fe-Si alloy + CsCl-FeSi [*Kuwayama et al.*, 2009], and the heavy dashed black line is the melting curve for FeSi from this study. The uncertainty in the melting curve is denoted by the light gray field.

functions recorded in the 14, 22, and 59 GPa melting experiments show smooth temperature increases and clear plateaus, but no evidence of discontinuities when passing through the suggested melting points of *Santamaría-Pérez and Boehler* [2008].

3.3. Geophysical Implications

3.3.1. FeSi in the D″ Layer

[20] *Knittle and Jeanloz* [1991] predicted that FeSi might occur in the D″ layer as a reaction product between the (Mg, Fe)SiO_3 perovskite or postperovskite of the lower mantle and the Fe alloy of the outer core. FeSi may also occur as a result of exsolution from the outer core during secular cooling [*Buffett et al.*, 2000]. Figure 7 is a depth versus temperature plot of the CMB region. The mantle adiabat is taken from *Katsura et al.* [2009] and assumes a lower mantle of pure $MgSiO_3$ perovskite. The broad range of core adiabats reflects the significant uncertainty in the melting point of iron at the ICB and is here bounded on the low-temperature side by the LH-DAC experiments of *Boehler* [1993] and on the high-temperature side by the ab initio molecular dynamics calculations of *Alfè* [2009]. The difference between the mantle and core adiabats yields a temperature jump across the CMB of between 1600 K and 3100 K. In reality, the geothermal gradient within D″ depends on the thermal transport properties and therefore on the composition of this layer. However, because there is still considerable uncertainty as to the nature of the lowermost mantle, we have simply interpolated linearly between the core and mantle adiabats. Between the solid black line (which represents the breakdown of hcp Fe-Si alloy → hcp Fe-Si alloy + CsCl-FeSi [*Kuwayama et al.*, 2009]) and the heavy dashed line (the melting curve of FeSi from this study), solid FeSi can occur. It is possible, therefore, that FeSi could be a stable component within a portion of the D″ layer, the thickness and depth of which would depend on the thermal gradient.

[21] For all but the lowest temperature core adiabats, FeSi will become molten toward the base of the D″ layer and throughout the outer core. If such melts were to form, their density would likely be intermediate between that of the core and mantle [*Caracas and Wentzcovitch*, 2004; *Dobson et al.*, 2003], causing them to pond at the CMB. Based on the 0 K calculations of *Caracas and Wentzcovitch* [2004], solid FeSi has a Vp ~14% lower than PREM and would be lower still for hot, molten FeSi. In combination with solid mantle silicates, liquid FeSi therefore has attributes that make it a possible candidate for a component of the partial melts postulated to explain the ultra-low velocity zones [*Lay et al.*, 2004].

3.3.2. FeSi in the Core

[22] Based on extrapolations to core conditions of the 300 K EOS of CsCl-FeSi [*Dobson et al.*, 2003], it is evident that the density of FeSi is too low to be the sole, or even the dominant, phase within the inner core, although based purely on this analysis a mixture of Fe and CsCl-FeSi is possible. However, assuming that silicon is the sole light element within the core, that nickel has little effect on phase relations, and that the system remains eutectic at the relevant conditions, the partitioning of silicon between the inner and outer cores depends on the composition of the eutectic. The multianvil data of *Kuwayama and Hirose* [2004] indicate the eutectic increases in silicon content with pressure to 26 wt% silicon at 21 GPa with the solidus located at ~2090 K, ~400 K below the melting point of pure iron. This suggests that any likely bulk core silicon content will fall on the iron-rich side of the eutectic, yielding an inner core consisting of an Fe-Si alloy and an outer core containing increasing amounts of silicon as secular cooling proceeds. The stability of Fe-Si alloys under high-pressure and high-temperature conditions

has been demonstrated in several recent in situ XRD studies in the LH-DAC. Fe-Si alloy in the hcp structure has been shown to be stable with 18.7 wt % Si up to 124 GPa at 300 K [*Hirao et al.*, 2004], 3.4 wt % Si up to 257 GPa and 3600 K [*Asanuma et al.*, 2008], 9.9 wt % Si up to ~130 GPa and ~2000 K [*Kuwayama et al.*, 2009], and 8 wt % Si up to ~170 GPa and ~3000 K [*Lin et al.*, 2009]. These studies also demonstrate that hcp Fe-Si alloy breaks down to a Si-poor hcp phase and a second Si-rich phase, either bcc structured Fe-Si alloy [*Lin et al.*, 2009] or CsCl-FeSi [*Kuwayama et al.*, 2009], and that the transition has a positive Clapeyron slope. However, extrapolations of these transitions to inner core conditions suggest that for likely Si contents, Si in the inner core is likely to be dissolved in an hcp Fe alloy. Thus CsCl-FeSi is unlikely to be present within the inner core. The possible presence of silicon in the outer core is enhanced by the similarity of the volumetric parameters [*Dobson et al.*, 2003] of CsCl-FeSi to PREM, while the high V_p values [*Badro et al.*, 2007] of CsCl-FeSi suggest that Si could serve to increase the V_p of pure iron toward that of the PREM model. Based on our melting data, the melting curve of pure iron [*Anderson and Isaak*, 2000; *Ma et al.*, 2004; *Shen et al.*, 1998, 2004] exceeds that of FeSi at ~165 GPa. Were the Fe-Si system to behave as a solid solution at high pressures, freezing at the ICB would still yield an inner core consisting of an Fe-rich alloy and an increasingly Si-rich liquid.

[23] **Acknowledgments.** We thank Andrew Jephcoat (DLS) for technical assistance in collecting the diffraction data. O.T.L. is grateful for financial support from a Natural Environment Research Council PhD studentship. This work was supported by Natural Environment Research Council grant NE/F019084/1 to M.J.W. Experiments at Bayreuth were funded by the European Commission through the Marie Curie Research Training Network "c2c" contract MRTN-CT-2006-035957.

References

Alfè, D. (2009), Temperature of the inner-core boundary of the Earth: Melting of iron at high pressure from first-principles coexistence simulations, *Phys. Rev. B*, *79*, 060101(R).

Allègre, C. J., J.-P. Poirier, E. Humler, and A. W. Hofmann (1995), The chemical composition of the Earth, *Earth Planet. Sci. Lett.*, *134*, 515–526, doi:10.1016/0012-821X(95)00123-T.

Anderson, O. L., and D. G. Isaak (2000), Calculating melting curves for phases of iron, *Am. Min.*, *85*, 376–385.

Asanuma, H., E. Ohtani, T. Sakai, H. Terasaki, S. Kamada, N. Hirao, N. Sata, and Y. Ohishi (2008), Phase relations of Fe-Si alloy up to core conditions: Implications for the Earth inner core, *Geophys. Res. Lett.*, *35*, L12307, doi:10.1029/2008GL033863.

Badro, J., G. Fiquet, F. Guyot, E. Gregoryanz, F. Occelli, D. Antonangeli, and M. d'Astuto (2007), Effect of light elements on the sound velocities in solid iron: Implications for the composition of Earth's core, *Earth Planet. Sci. Lett.*, *254*, 233–238, doi:10.1016/j.epsl.2006.11.025.

Boehler, R. (1993), Temperatures in the Earth's core from melting-point measurements of iron at high static pressures, *Nature*, *363*, 534–536, doi:10.1038/363534a0.

Boehler, R. (2000), High-pressure experiments and the phase diagram of lower mantle and core materials, *Rev. Geophys.*, *38*, 221–245, doi:10.1029/1998RG000053.

Boehler, R., N. von Bargen, and A. Chopelas (1990), Melting, thermal expansion, and phase transitions of iron at high pressures, *J. Geophys. Res.*, *95*, 21,731–21,736, doi:10.1029/JB095iB13p21731.

Boehler, R., M. Ross, and D. B. Broecker (1997), Melting of LiF and NaCl to 1 Mbar: Systematics of ionic solids at extreme conditions, *Phys. Rev. Lett.*, *78*(24), 4589–4592, doi:10.1103/PhysRevLett.78.4589.

Buffett, B. A., E. J. Garnero, and R. Jeanloz (2000), Sediments at the top of Earth's core, *Science*, *290*, 1338–1342, doi:10.1126/science.290.5495.1338.

Caracas, R., and R. Wentzcovitch (2004), Equation of state and elasticity of FeSi, *Geophys. Res. Lett.*, *31*, L20603, doi:10.1029/2004GL020601.

Dewaele, A., M. Mezouar, N. Guignot, and P. Loubeyre (2007), Melting of lead under high pressure studied using second-scale time-resolved x-ray diffraction, *Phys. Rev. B*, *76*, 144106, doi:10.1103/PhysRevB.76.144106.

Dobson, D. P., L. Vocadlo, and I. G. Wood (2002), A new high-pressure phase of FeSi, *Am. Min.*, *87*, 784–787.

Dobson, D. P., W. A. Chrichton, P. Bouvier, L. Vocadlo, and I. G. Wood (2003), The equation of state of CsCl-structured FeSi at 40 GPa: Implications for silicon in Earth's core, *Geophys. Res. Lett.*, *30*(1), 1014, doi:10.1029/2002GL016228.

Dziewonski, A. M., and D. L. Anderson (1981), Preliminary reference Earth model, *Phys. Earth Planet. Inter.*, *25*, 297–356, doi:10.1016/0031-9201(81)90046-7.

Fitoussi, C., B. Bourdon, T. Kleine, F. Oberli, and B. C. Reynolds (2009), Si isotope systematics of meteorites and terrestrial peridotites: Implications for Mg/Si fractionation in the solar nebula and for Si in the Earth's core, *Earth Planet. Sci. Lett.*, *287*, 77–85, doi:10.1016/j.epsl.2009.07.038.

Georg, R. B., A. N. Halliday, E. A. Schauble, and B. C. Reynolds (2007), Silicon in the Earth's core, *Nature*, *447*, 1102–1106, doi:10.1038/nature05927.

Gessman, C. K., B. J. Wood, D. C. Rubie, and M. R. Kilburn (2001), Solubility of silicon in liquid metal at high pressure: Implications for the composition of the Earth's core, *Earth Planet. Sci. Lett.*, *184*, 367–376, doi:10.1016/S0012-821X(00)00325-3.

Goarant, F., F. Guyot, J. Peyronneau, and J. P. Poirier (1992), High-pressure and high-temperature reactions between silicates and liquid-iron alloys, in the diamond anvil cell, studied by analytical electron microscopy, *J. Geophys. Res.*, *97*(B4), 4477–4487, doi:10.1029/92JB00018.

Guyot, F., J. H. Zhang, I. Martinez, J. Matas, Y. Ricard, and M. Javoy (1997), P-V-T measurements of iron silicide (epsilon-FeSi): Implications for silicate-metal interactions in the early Earth, *Eur. J. Min.*, *9*(2), 277–285.

Hammersley, A. P. (1997), FIT2D: An introduction and overview, *Tech. Rep. ESRF-97-HA-02T*, ESRF, Grenoble, France.

Helffrich, G., and S. Kaneshima (2004), Seismological constraints on core composition from Fe-O-S liquid immiscibility, *Science*, *306*, 2239–2242.

Hirao, N., E. Ohtani, T. Kondo, and T. Kikegawa (2004), Equation of state of iron-silicon alloys to megabar pressure, *Phys. Chem. Miner.*, *31*, 329–336, doi:10.1007/s00269-004-0387-x.

Katsura, T., et al. (2009), P-V-T relations of $MgSiO_3$ perovskite determined by in situ X-ray diffraction using a large-volume high-pressure apparatus, *Geophys. Res. Lett.*, *36*, L01305, doi:10.1029/2008GL035658.

Knittle, E., and R. Jeanloz (1991), Earth's core-mantle boundary: Results of experiments at high pressures and temperatures, *Science*, *251*, 1438–1443, doi:10.1126/science.251.5000.1438.

Knittle, E., and Q. Williams (1995), Static compression of ε-FeSi and an evaluation of reduced silicon as a deep Earth constituent, *Geophys. Res. Lett.*, *22*(4), 445–448, doi:10.1029/94GL03346.

Kuwayama, Y., and K. Hirose (2004), Phase relations in the system Fe-FeSi at 21 GPa, *Am. Min.*, *89*, 273–276.

Kuwayama, Y., T. Sawai, K. Hirose, N. Sata, and Y. Ohishi (2009), Phase relations of iron-silicon alloys at high pressure and temperature, *Phys. Chem. Miner.*, *36*, 511–518, doi:10.1007/s00269-009-0296-0.

Lacaze, J., and B. Sundman (1991), An assessment of the Fe-C-Si system, *Metall. Trans. A*, *22*, 2211–2223, doi:10.1007/BF02664987.

Lay, T., E. J. Garnero, and Q. Williams (2004), Partial melting in a thermo-chemical boundary layer at the base of the mantle, *Phys. Earth Planet. Inter.*, *146*, 441–467, doi:10.1016/j.pepi.2004.04.004.

Lazor, P., G. Shen, and S. K. Saxena (1993), Laser-heated diamond anvil cell experiments at high pressure: Melting curve of nickel up to 700 kbar, *Phys. Chem. Miner.*, *20*, 86–90, doi:10.1007/BF00207200.

Lin, J.-F., A. J. Campbell, D. L. Heinz, and G. Shen (2003), Static compression of iron-silicon alloys: Implications for silicon in the Earth's core, *J. Geophys. Res.*, *108*(B1), 2045, doi:10.1029/2002JB001978.

Lin, J.-F., H. P. Scott, R. A. Fischer, Y.-Y. Chang, I. Kantor, and V. B. Prakapenka (2009), Phase relations of Fe-Si alloy in Earth's core, *Geophys. Res. Lett.*, *36*, L06306, doi:10.1029/2008GL036990.

Lord, O. T., M. J. Walter, R. Dasgupta, D. Walker, and S. M. Clark (2009), Melting in the Fe-C system to 70 GPa, *Earth Planet. Sci. Lett.*, *284*, 157–167, doi:10.1016/j.epsl.2009.04.017.

Ma, Y., M. Somayazulu, G. Shen, H.-K. Mao, J. Shu, and R. J. Hemley (2004), In situ x-ray diffraction studies of iron to Earth-core conditions, *Phys. Earth Planet. Inter.*, *143–144*, 455–467, doi:10.1016/j.pepi.2003.06.005.

Mao, H. K., J. Xu, and P. M. Bell (1986), Calibration of the ruby pressure gauge to 800 Kbar under quasi-hydrostatic conditions, *J. Geophys. Res.*, *91*, 4673–4676, doi:10.1029/JB091iB05p04673.

Mossenfelder, J. L., J. A. D. Connolly, D. C. Rubie, and M. Liu (2000), Strength of (Mg,Fe)SiO4 wadsleyite determined by relaxation of transformation stress, *Phys. Earth Planet. Inter.*, *120*, 63–78, doi:10.1016/S0031-9201(00)00142-4.

Poirier, J. P. (1994), Light elements in the Earth's outer core--A critical review, *Phys. Earth Planet. Inter.*, *85*, 319–337, doi:10.1016/0031-9201(94)90120-1.

Ringwood, A. E., and W. Hibberson (1990), The system Fe-FeO revisited, *Phys. Chem. Miner.*, *17*, 313–319, doi:10.1007/BF00200126.

Sakai, T., T. Kondo, E. Ohtani, H. Terasaki, N. Endo, T. Kuba, T. Suzuki, and T. Kikegawa (2006), Interaction between iron and post-perovskite at core-mantle boundary and core signature in plume source region, *Geophys. Res. Lett.*, *33*, L15317, doi:10.1029/2006GL026868.

Sanloup, C., F. Guyot, P. Gillet, and Y. Fei (2002), Physical properties of liquid Fe alloys at high pressure and their bearings on the nature of metallic planetary cores, *J. Geophys. Res.*, *107*(B11), 2272, doi:10.1029/2001JB000808.

Santamaría-Pérez, D., and R. Boehler (2008), FeSi melting curve up to 70 GPa, Earth Planet. *Sci. Lett.*, *265*, 743–747, doi:10.1016/j.epsl.2007.11.008.

Shahar, A., K. Ziegler, E. D. Young, A. Ricolleau, E. A. Schauble, and Y. Fei (2009), Experimentally determined Si isotope fractionation between silicate and Fe metal and implications for Earth's core formation, *Earth Planet. Sci. Lett.*, *288*, 228–234, doi:10.1016/j.epsl.2009.09.025.

Shen, G., and P. Lazor (1995), Measurement of melting temperatures of some minerals under lower mantle pressures, *J. Geophys. Res.*, *100*(B9), 17,699–17,713, doi:10.1029/95JB01864.

Shen, G., P. Lazor, and S. K. Saxena (1993), Melting of wüstite and iron up to pressures of 600 kbar, *Phys. Chem. Miner.*, *20*, 91–96, doi:10.1007/BF00207201.

Shen, G., H.-K. Mao, and R. J. Hemley (1998), Melting and crystal structure of iron at high pressures and temperatures, *Geophys. Res. Lett.*, *25*(3), 373–376, doi:10.1029/97GL03776.

Shen, G., M. L. Rivers, S. R. Sutton, N. Sata, V. B. Prakapenka, J. Oxley, and K. S. Suslick (2004), The structure of amorphous iron at high pressures to 67 GPa measured in a diamond anvil cell, *Phys. Earth Planet. Inter.*, *143–144*, 481–495, doi:10.1016/j.pepi.2003.05.004.

Takafuji, N., K. Hirose, M. Mitome, and Y. Bando (2005), Solubilities of O and Si in liquid iron in equilibrium with (Mg,Fe)SiO_3 perovskite and the light elements in the core, *Geophys. Res. Lett.*, *32*, L06313, doi:10.1029/2005GL022773.

Vocadlo, L., G. D. Price, and I. G. Wood (1999), Crystal structure, compressibility and possible phase transitions in ε-FeSi studied by first-principles pseudopotential calculations, *Acta Crystallogr., Sect. B Struct. Sci.*, *55*, 484–493, doi:10.1107/S0108768199001214.

Vocadlo, L., K. S. Knight, G. D. Price, and I. G. Wood (2002), Thermal expansion and crystal structure of FeSi between 4 and 1173 K determined by time-of-flight neutron powder diffraction, *Phys. Chem. Miner.*, *29*, 132–139, doi:10.1007/s002690100202.

Walter, M. J., and K. T. Koga (2004), The effects of chromatic dispersion on temperature measurement in the laser-heated diamond anvil cell, *Phys. Earth Planet. Inter.*, *143–144*, 541–558, doi:10.1016/j.pepi.2003.09.019.

L. Armstrong, O. T. Lord, and M. J. Walter, Department of Earth Sciences, University of Bristol, Wills Memorial Building, Queen's Road, Bristol BS8 1RJ, UK. (Oliver.Lord@bristol.ac.uk)

S. M. Clark, Advanced Light Source, Lawrence Berkeley National Laboratory, MS6R2100, 1 Cyclotron Road, Berkeley, CA 94720-8226, USA.

D. P. Dobson, Department of Earth Sciences, University College London, Gower Street, London WC1E 6BT, UK.

A. Kleppe, Diamond Light Source Ltd., Diamond House, Harwell Science and Innovation Campus, Didcot OX110 DE, UK.